Tactile Sensor for Minimally Invasive Surgery Using Electrical Impedance Tomography

James Avery, *Member, IEEE*, Darya Shulakova, Mark Runciman, *Graduate Student Member, IEEE*, George P. Mylonas, *Member, IEEE*, and Ara Darzi, *Member, IEEE*

***Abstract*—Whilst offering numerous benefits to patients, minimally invasive surgery (MIS) has a disadvantage in the loss of tactile feedback to the surgeon, traditionally offering valuable qualitative tissue assessment, such as tumour identification and localisation. Tactile sensors aim to overcome this loss of sensation by detecting tissue characteristics such as stiffness, composition and temperature. Tactile sensors have previously been incorporated into MIS robotic end effectors, which require lengthy scanning procedures due to localised sensitivity. Distributed tactile sensors, or "artificial skin" offer a map of tissue properties in a single instance but are often not suitable for MIS applications due to limited biocompatibility or large collapsed volumes. We propose a deployable, soft, tactile sensor with a deformable saline chamber and integrated Electrical Impedance Tomography (EIT) electrodes. During contact with tissue, the saline is displaced from the chamber and the lesion size and stiffness can be inferred from the resultant impedance changes. Through optimisation of the EIT measurement protocol and hardware the sensor was capable of localising the centre of mass of palpation targets within 1.5 mm in simulation and 2.3–4.6mm in phantom experiments. Reconstructed image metrics differentiated target objects from 8–30 mm.**

***Index Terms*—Electrical impedance tomography, medical robotics, soft robotics, tactile sensors.**

I. Introduction

The advent of minimally invasive surgery (MIS) has provided many benefits to patients over open surgery due to smaller incisions made by the surgeon, resulting in faster healing and recovery time. However, despite the numerous benefits, MIS has brought a loss of tactile 'feel' to the surgeon. Tactile or haptic feedback provides information of the shape, stiffness and texture of the organ or tissue to the surgeon's hands through the sense of touch. This enables a surgeon to identify tumours, through palpation, which exhibit a 'tougher' feel than healthy soft tissue, pulse felt from blood vessels, and abnormal lesions. Tactile sensors have been fabricated to be able to sense different characteristics of tissue inside the body such through physical touch. Sensor outputs include: shape, size, pressure, softness, composition, temperature, vibration, shear and normal forces [1]. Tactile transduction mechanisms in the literature include capacitive, inductive, piezoelectric, piezoresistive, magnetic and optical [2].

Numerous approaches to tactile sensing specific to MIS have been explored, typically at the tip of the robot end effector [3]. The localised sensitivity of these sensors necessitates time consuming scanning procedures to build a map for assessment. Conversely, distributed sensing typically focuses on the creation of "artificial skin" for robotics and are often not suitable for MIS due to lack of biocompatibility and large volumes when collapsed [4]. It is possible to obtain measures of elastic properties through pressure and volume curves during balloon inflation [5]. However, there is ambiguity with a single measurement, as it is not possible to ascertain which area of the tissue under the balloon is deforming.

Manuscript received July 23, 2020; revised September 10, 2020; accepted October 11, 2020. Date of publication October 16, 2020; date of current version November 20, 2020. This article was recommended for publication by Associate Editor K. Cleary and Editor P. Dario upon evaluation of the reviewers' comments. This work was supported by the National Institute for Health Research (NIHR) Imperial Biomedical Research Centre (BRC). *(Corresponding author: James Avery.)*

The authors are with the Department of Surgery and Cancer, Imperial College London, W2 1NY, U.K., and also with the Hamlyn Centre, Institute of Global Health Innovation, Imperial College, London SW7 2AZ, U.K. (e-mail: james.avery@imperial.ac.uk).

Digital Object Identifier 10.1109/TMRB.2020.3031636

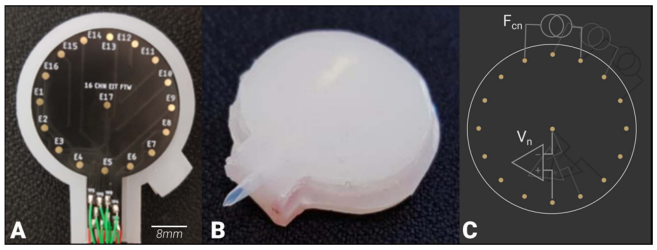

Fig. 1. Soft tactile EIT sensor design (A) FPC affixed to base layer of sensing chamber (B) Complete sensor with encapsulated chamber with hydraulic inlet (C) EIT concept: current injected between pairs of electrodes and voltages measured between all electrodes and central ground.

To address these limitations, we are proposing a deployable, soft, tactile sensor based on Electrical Impedance Tomography (EIT). The deformation of a saline filled chamber is measured using multiple impedance measurements, and thus the size and stiffness of the contact tissue can be inferred. The majority of impedance based tactile sensors are constructed of thin sheets, which can be approximated to 2D EIT problems [6], however measuring the deformation of the volume of the saline chamber necessitates a full 3D image reconstruction. We present optimisations of the measurement configurations and investigate candidate metrics from images and from phantom experiments.

II. Materials and Methods

A. Sensor Design

The sensor, Fig. 1, was constructed from two layers of Polydimethylsiloxane (PDMS): a DragonSkin 30 base layer, and a 2mm Eco-Flex 50 top layer. A Flexible Printed Circuit (FPC) with a ring of 16 electrodes spaced equally at a radius of 15 mm from a central ground electrode was affixed to the base layer using SilPoxy adhesive. Finally, a silicone tube with 2 mm inner diameter was connected to the base as a hydraulic inlet, and the two layers were sealed using SilPoxy. To deploy, the sensor chamber was filled with 0.2% saline as the conductive medium for EIT measurements. Deformation of the domed PDMS surface of the sensor by an object would locally displace saline at the contact point and create a localised impedance change. By combining a multitude of impedance measurements, Fig. 1C, an EIT image of the apparent conductivity change could be reconstructed, and the target location and size inferred from the result.

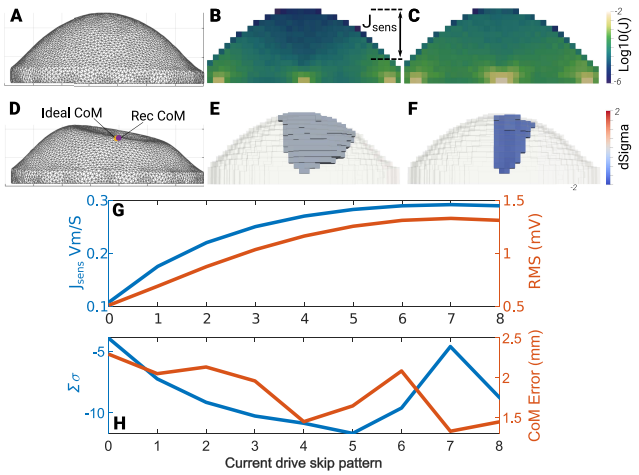

Fig. 2. EIT sensing optimisation (A) FEM of sensing chamber. Measurement sensitivity with (B) skip-0 and (C) skip-8 patterns. (D) Simulated deformation and CoM comparison. Resultant EIT images for (E) skip-0 and (F) skip-8. (G) RMS voltage change δV and total sensitivity in sensing chamber J_{sens} (H) Reconstructed centre of mass error and total conductivity change $\Sigma\sigma$.

B. EIT Hardware

A Frequency Division Multiplexed EIT (FDM-EIT) system used in previous studies [7] was extended to provide a maximum of 18 current injections, using three daisy chained boards of six independent Howland current sources [8]. A National Instruments USB-6363 16-bit Data acquisition (DAQ) was used to record the voltages with 50 kHz sample rate on all 16 electrodes on the outer ring, with respect to the central ground. The voltage amplitude on each electrode at each frequency was obtained from the FFT, to provide a full data frame of 256 measurements.

Current was injected at sixteen frequencies, from 2.75 to 13.625 kHz at 725 Hz spacing. These were chosen to give a clearance of 150 Hz between all harmonics of the carrier frequencies to reduce. A current amplitude of 120 μA, far below the IEC 60601 safety standards, was injected at all frequencies, resulting in voltages of approximately 200 mV. The theoretical maximum frame rate was 725 Hz based on the frequency spacing, however a minimum of 1000 samples (or 50 Hz) was needed to obtain maximum Signal to Noise Ratio (SNR).

C. EIT Imaging

The EIT software used in this study was a fork of the common EIDORS package [9] and the meshing and reconstruction methods developed by Aristovich *et al.* [10]. The EIT forward problem was solved using a Finite Element Mesh (FEM) based on a CAD model of the internal chamber of the inflated sensor, Fig. 2A, created using custom meshing software. The mesh was refined around each electrode by a factor of 10 within a region of 0.8 mm. Conductivity images were reconstructed using Zeroth Order Tikhonov regularisation using cross-validation to select the hyper parameter λ. The forward FEM consistent of 310k tetrahedral elements, and a hexahedral mesh of 7k elements was used for reconstruction. In all EIT images the area of deformation corresponded to a reconstructed volume of decreased conductivity. For analysis, the perturbation was defined as the largest contiguous cluster of elements with at least 75% of the maximum absolute reconstructed change.

III. Experimental Setup

A. EIT Protocol Optimisation

The sequence of electrodes used for current stimulation and voltage measurements, or EIT "protocol", is crucial in determining the overall sensitivity. As the optimal protocol is highly application specific, a simulation study was performed to find the protocol which maximised the sensitivity in the entirety of the sensing chamber J_{sens}, voltage change δV, and image quality. As the voltage measurement pattern is fixed by the DAQ, only the effect of the current injection pattern was investigated. For approximately circular electrode configurations, these are known as "skip patterns", based on the number of passive electrodes between injecting electrodes, e.g., Fig. 1C depicts a skip-1 pattern [11]. To obtain an example change in voltage, the EIT forward model was calculated with a deformed version of the original CAD model Fig. 2D. Image quality was assessed by calculating the total conductivity change within the perturbation $\Sigma\sigma$ and weighted centre of mass (CoM) error was used to assess localisation accuracy.

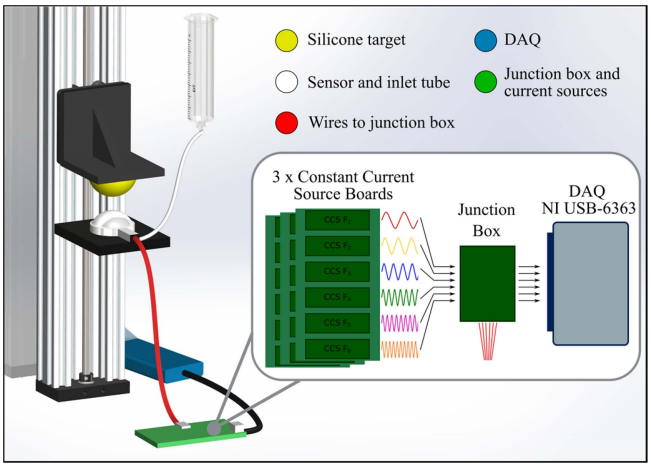

Fig. 3. Palpation test setup. Silicone targets compressed onto the EIT sensor using a linear stage. Insert: FDM-EIT system overview.

B. EIT Hardware

To assess the new current source and the impact of the connection of multiple circuit boards, measurements were made on a custom resistor phantom of 2 kΩ load. Data were collected for 60 s with all 16 current sources active. To prevent biasing the reconstruction towards the channels with lower noise, an FDM-EIT system must have frequency invariant SNR performance. This was assessed in these measurements by testing for statistical significance in SNR across frequencies. To assess the suitability of the electroless nickel immersion gold (ENIG) surface of the FPC electrodes, measurements of the noise were collected using a single isolated current source, at frequencies between 1 and 20 kHz in 1 kHz increments.

C. Palpation Test

A PDMS target was attached to the gantry of a linear stage with a resolution of 0.01 mm, which moved at a constant speed of 25 mm/s, while the sensor was affixed to a stationary rigid plate such that the silicone targets deformed the top surface of the sensor, Fig. 3. The hydraulic inlet tube was connected to a reservoir elevated above the sensor whose free surface was allowed to move when fluid was displaced from the sensor. Targets of 8-30mm radii, approximating tumours, were compressed onto the sensor, compensating the initial distance between sensor and target. EIT images were reconstructed at 50 Hz frame rate after subtraction of the initial steady state values.

IV. Results

A. EIT Protocol Optimisation

The sensitivity within the sensing volume J_{sens} increased with skip pattern, with a corresponding increase in detected voltage change, as

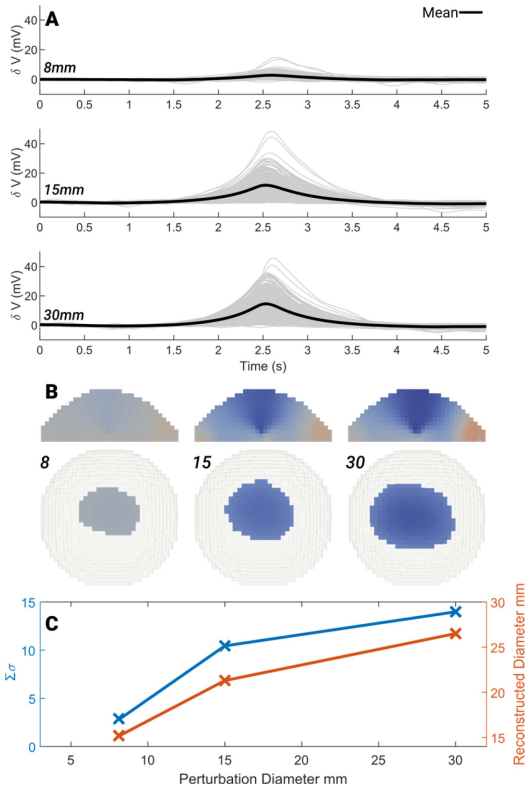

Fig. 4. Palpation results for 8, 15 and 30mm targets (A) Voltage changes with mean δV highlighted (B) reconstructed perturbations of maximum change (C) Image metrics: object diameter (red) and total conductivity change $\Sigma\sigma$ (blue).

shown in Fig. 2. This is also evident in the improved reconstruction (Fig. 2E compared to Fig. 2F) and greater $\Sigma\sigma$. The CoM error was less than 1.5 mm for skip patterns 7 and 8. Given the decrease in reconstructed intensity using skip-7, skip-8 was chosen as a trade-off between these metrics for subsequent experiments.

B. EIT Hardware

The SNR measured on the resistor phantom was 66.8 $\pm$ 7.3 dB, and there was no significant difference in SNR below 13 kHz (P = 0.286 One-way ANOVA). There was a decrease in SNR at the highest frequency (13.625 kHz) although this was not found to be significant (P = 0.528). Using the FPC electrodes, the SNR increased to 74.2 $\pm$ 8.3 dB and showed a similar stability across frequency. With no significant changes in SNR (ANOVA), except at 20 kHz, the highest frequency, which decreased from the mean by 23 dB.

C. Palpation Test

The maximum change in voltage, Fig. 4A, increased with target object size, with a corresponding increase in reconstructed intensity, Fig. 4B. The conductivity changes $\Sigma\sigma$ demonstrated an approximately linear increase with object size. However, the average reconstructed diameter substantially overestimated the 5- and 15-mm objects. The CoM localisation in the XY directions ranged from 2.3–4.6 mm across all frames. However, the Z localisation accuracy was significantly compromised by artefactual changes close to the electrodes.

V. Conclusion

This decrease in spatial resolution with distance from the boundary electrodes is typical of EIT based sensors. Reducing the point spread function of the reconstruction would improve the localisation accuracy and shape estimation. This could be achieved through reconfiguration of the FPC to include internal electrodes [12], [13], [14] or a full grid [10], [15], [16] to better distribute the sensitivity across the plane of the electrodes. However, these may not sufficiently address the decrease in out of plane sensitivity towards the deformable contact surface. Potential solutions to this problem are to further increase the SNR of the system to ensure these small changes still detected, or improved reconstruction algorithms targeting this problem [17], [18]. Placing electrodes onto the deformable surface would greatly increase the sensitivity. However, the voltage changes observed would then be as a result of both boundary deformation and electrode movement, making the images challenging to reconstruct and interpret.

Using FPCs to create the electrode arrays allowed for accurate electrode placement and simple integration into the sensor body. Using saline as a conductive medium as opposed to a conductive elastomer meant the challenges of connecting rigid electrodes to the flexible substrates were avoided [19], [20]. However, the disadvantage of this approach is that the polyimide substrate is not stretchable, and thus limits the collapsibility of the sensor. Using Magnetic Resonance conditional materials once an optimal configuration was found would enable a wider range of surgical applications. The extent to which the PDMS encapsulation insulates the sensor from electrical and thermal interference from surgical instruments like radiofrequency ablation or diathermy requires experimental investigation and may necessitate additional data processing prior to reconstruction.

There was no substantial decrease in SNR as a result of daisy chaining three parallel current sources, and the FPC electrodes and improved hardware increased SNR by 8 dB compared to previous implementations [7]. The decrease at 20 kHz is caused by the DAQ anti-aliasing filter and represents the upper limit of the carrier frequency. This provides a total bandwidth of 19 kHz, which would allow for a maximum of 25 current injections with this same frequency spacing of 725 Hz. Any sensors requiring a larger protocol would consequently require a decrease in frame rate, or a faster DAQ, to avoid decreasing SNR. The FDM allows for higher frame rates and simpler processing, but the disadvantage is that the hardware prevents the use of dynamic protocols, which could improve image quality by targeting the deformed volume once a perturbation has been identified [21].

Currently the results are uncalibrated, so measurements of lesion size or tissue properties are only relative quantities. Extension of the phantom tests within this study to a full XYZ map, would provide a dataset to create a localisation map for machine learning approaches [12], in combination with a denoising/post-processing step have been successfully applied to 2D tactile sensors [6]. It may also be possible to obtain a similar transform based on simulations of the deformation of the sensor in SOFA [22]. Ultimately it may be possible to create a joint physics simulation, combining EIT and mechanical models, and thus calculate the deformation directly.

Experiments are ongoing to find the optimal metric, either from voltage traces or images, to quantify the elastic properties of the contact tissue and potentially create elastography images across the sensor surface. The results show a proof of concept for this sensor but demonstrate the importance of correct metric choice and calibration to obtain clinically useful results.

References

[1] M. I. Tiwana, S. J. Redmond, and N. H. Lovell, "A review of tactile sensing technologies with applications in biomedical engineering," *Sens. Actuat. A, Phys.*, vol. 179, pp. 17–31, Jan. 2012, doi: 10.1016/j.sna.2012.02.051.

[2] J. Tegin and J. Wikander, "Tactile sensing in intelligent robotic manipulation—A review," *Ind. Rob.*, vol. 32, no. 1, pp. 64–70, 2005, doi: 10.1108/01439910510573318.
[3] P. Puangmali, K. Althoefer, L. D. Seneviratne, D. Murphy, and P. Dasgupta, "State-of-the-art in force and tactile sensing for minimally invasive surgery," *IEEE Sensors J.*, vol. 8, no. 4, pp. 371–380, Apr. 2008, doi: 10.1109/JSEN.2008.917481.
[4] K. Liu *et al.*, "Artificial sensitive skin for robotics based on electrical impedance tomography: A review," *Adv. Intell. Syst.*, vol. 2, Apr. 2020, Art. no. 1900161, doi: 10.1002/aisy.201900161.
[5] Y. Tanaka *et al.*, "Development of a real-time tactile sensing system for brain tumor diagnosis," *Int. J. Comput. Assist. Radiol. Surg.*, vol. 5, no. 4, pp. 359–367, Jul. 2010, doi: 10.1007/s11548-010-0426-7.
[6] X. Duan, S. Taurand, and M. Soleimani, "Artificial skin through super-sensing method and electrical impedance data from conductive fabric with aid of deep learning," *Sci. Rep.*, vol. 9, no. 1, pp. 1–11, 2019, doi: 10.1038/s41598-019-45484-6.
[7] J. Avery, M. Runciman, A. Darzi, and G. P. Mylonas, "Shape sensing of variable stiffness soft robots using electrical impedance tomography," in *Proc. Int. Conf. Robot. Autom. (ICRA)*, vol. 2019. Montreal, QC, Canada, May 2019, pp. 9066–9072, doi: 10.1109/ICRA.2019.8793862.
[8] J. Avery, T. Dowrick, A. Witkowska-Wrobel, M. Faulkner, K. Aristovich, and D. Holder, "Simultaneous EIT and EEG using frequency division multiplexing," *Physiol. Meas.*, vol. 40, no. 3, Apr. 2019, Art. no. 034007, doi: 10.1088/1361-6579/ab0bbc.
[9] A. Adler and W. R. B. Lionheart, "Uses and abuses of EIDORS: An extensible software base for EIT," *Physiol. Meas.*, vol. 27, no. 5, pp. S25–S42, May 2006, doi: 10.1088/0967-3334/27/5/S03.
[10] K. Y. Aristovich, G. S. dos Santos, B. C. Packham, and D. S. Holder, "A method for reconstructing tomographic images of evoked neural activity with electrical impedance tomography using intracranial planar arrays," *Physiol. Meas.*, vol. 35, no. 6, pp. 1095–1109, Jun. 2014, doi: 10.1088/0967-3334/35/6/1095.
[11] A. Adler, P. O. Gaggero, and Y. Maimaitijiang, "Adjacent stimulation and measurement patterns considered harmful," *Physiol. Meas.*, vol. 32, no. 7, pp. 731–744, Jul. 2011, doi: 10.1088/0967-3334/32/7/S01.
[12] H. Lee, K. Park, J. Kim, and K. J. Kuchenbecker, "Internal array electrodes improve the spatial resolution of soft tactile sensors based on electrical resistance tomography," in *Proc. IEEE Int. Conf. Robot. Autom.*, Montreal, QC, Canada, May 2019, pp. 5411–5417, doi: 10.1109/ICRA.2019.8794276.
[13] D. S. Tawil, D. Rye, and M. Velonaki, "Improved image reconstruction for an EIT-based sensitive skin with multiple internal electrodes," *IEEE Trans. Robot.*, vol. 27, no. 3, pp. 425–435, Jun. 2011, doi: 10.1109/TRO.2011.2125310.
[14] R. Li, Z. Hao, W. Mu, and X. Wang, "Optimal design of electrodes for an electrical impedance tomography based flexible sensor," in *Proc. Sens. Smart Struct. Technol. Civil Mech. Aerosp. Syst.*, Mar. 2019, p. 102, doi: 10.1117/12.2513812.
[15] E. J. Lee *et al.*, "Design of a microscopic electrical impedance tomography system for 3D continuous non-destructive monitoring of tissue culture," *Biomed. Eng. Online*, vol. 13, no. 1, pp. 1–15, 2014, doi: 10.1186/1475-925X-13-142.
[16] M. Faulkner, S. Hannan, K. Aristovich, J. Avery, and D. Holder, "Feasibility of imaging evoked activity throughout the rat brain using electrical impedance tomography," *Neuroimage*, vol. 178, pp. 1–10, Sep. 2018, doi: 10.1016/j.neuroimage.2018.05.022.
[17] Y. Yang, J. Jia, S. Smith, N. Jamil, W. Gamal, and P.-O. Bagnaninchi, "A miniature electrical impedance tomography sensor and 3-D image reconstruction for cell imaging," *IEEE Sensors J.*, vol. 17, no. 2, pp. 514–523, Jan. 2017, doi: 10.1109/JSEN.2016.2631263.
[18] Y. Wang, S. Ren, and F. Dong, "Focusing sensor design for open electrical impedance tomography based on shape conformal transformation," *Sensors*, vol. 19, no. 9, p. 2060, May 2019, doi: 10.3390/s19092060.
[19] E. Cuttaz et al., "Conductive elastomer composites for fully polymeric, flexible bioelectronics," *Biomater. Sci.*, vol. 7, no. 4, pp. 1372–1385, 2019, doi: 10.1039/c8bm01235k.
[20] J.-B. Chossat, H.-S. Shin, Y.-L. Park, and V. Duchaine, "Soft tactile skin using an embedded ionic liquid and tomographic imaging," *J. Mech. Robot.*, vol. 7, no. 2, May 2015, Art. no. 021008, doi: 10.1115/1.4029474.
[21] S. Russo, S. Nefti-Meziani, N. Carbonaro, and A. Tognetti, "A quantitative evaluation of drive pattern selection for optimizing EIT-based stretchable sensors," *Sensors (Switzerland)*, vol. 17, no. 9, pp. 1–16, 2017, doi: 10.3390/s17091999.
[22] E. Coevoet, A. Escande, and C. Duriez, "Optimization-based inverse model of soft robots with contact handling," *IEEE Robot. Autom. Lett.*, vol. 2, no. 3, pp. 1413–1419, Jul. 2017, doi: 10.1109/LRA.2017.2669367.